Atmospheric Research 166 (2015) 195–203

Contents lists available at ScienceDirect

Atmospheric Research

journal homepage: www.elsevier.com/locate/atmos

Invited critical review

The Earth's energy balance

Graeme L. Stephens [a,b,*], Tristan L'Ecuyer [c]

[a] Jet Propulsion Laboratory, California Institute of Technology, 4800 Oak Grove Drive, Pasadena, CA 91109, USA
[b] Department of Meteorology, University of Reading, UK
[c] Department of Atmospheric Sciences, University of Wisconsin, Madison, WI 80523, USA

ARTICLE INFO

Article history:
Received 17 November 2014
Received in revised form 22 June 2015
Accepted 26 June 2015
Available online 2 July 2015

ABSTRACT

This paper reviews the status of our understanding of the Earth's annual, global mean energy balance, the hemispheric energy balances and the symmetry observed about the equator, and explores the influence of latitudinal changes of energy both on the annual mean and seasonal transports of energy from low latitudes to higher latitudes. Based on the best available information we show that our planet continues to be out of balance with additional heat being added to it at the rate of $0.6 \pm 0.4\ \mathrm{Wm}^{-2}$. This heat appears to be taken up primarily by the oceans of the SH and perhaps mostly equatorward of 37 S. The nature of the adjustments applied to our best estimates of individual, annual mean fluxes of energy to produce a balance are described and the results of applying a more formal constraint for these adjustments are discussed. The energy balances of the Southern and Northern Hemispheres are then shown to be practically identical which in turn suggests the transport of energy across the equator in the net is close to zero. In fact the hemispheres are not identically symmetrical with the SH being slightly out of balance absorbing the additional heat and transporting a small amount of net heat across the equator to the balanced NH. The symmetry in absorbed solar and the near symmetry in OLR are remarkable in their own right and are a result of the effects of clouds both on solar reflection and OLR that act to offset land–ocean interhemispheric differences. We then demonstrate important interhemispheric seasonal influences on the heat transported to the winter pole that conspire to make these seasonal transports lopsided. This asymmetry is a direct result of the eccentricity of the Earth's orbit that induces larger energy losses from the southern winter hemisphere. This in turn produces a latitudinal asymmetry in the location of on the tropical trough zone, a region from which energy is always moved to the winter pole, requiring it be located deeper into the NH.

Contents

1. Introduction

The Earth's climate is determined by the flows (fluxes) of energy into and out of the planet and to and from the Earth's surface. The geographical distributions of these fluxes are particularly important. The latitudinal

* Corresponding author at: Jet Propulsion Laboratory, California Institute of Technology, 4800 Oak Grove Drive, Pasadena, CA 91109, USA.

http://dx.doi.org/10.1016/j.atmosres.2015.06.024
0169-8095/

variation of the top of the atmosphere (TOA) fluxes establishes one of the most fundamental aspects of Earth's climate determining how much heat is transported from low latitudes to high latitudes (e.g., VonderHaar and Oort, 1973; Stone, 1978; Donohoe and Battisti, 2012 among many others). The further disposition of net TOA energy between the atmosphere and surface is also of fundamental relevance to climate. The surface energy fluxes are fundamental to understanding the carbon, energy and water nexus. Surface energy fluxes drive ocean circulations, determine how much water is evaporated from the Earth's surface, and govern the planetary hydrological cycle (e.g., Wild and Leipert, 2010). Changes to the surface energy balance also ultimately control how this hydrological cycle responds to the small energy imbalances that force climate change (Allen and Ingram, 2002; Andrews, 2009; Stephens and Hu, 2010; O'Gorman et al., 2012).

Despite the fundamental importance of the energy balance to our understanding of climate and climate change, there still remain a number of challenges in quantifying it globally and in understanding its behavior regionally. Current depictions of the global surface energy balance (e.g., Stephens et al., 2012a) indicate that uncertainties attached to our best depiction of the net surface energy balance are an order of magnitude larger than the small imbalance of 0.64 ± 0.43 Wm^{-2} inferred from the ocean heat content (OHC) changes (Llovel et al., 2014) and from observed TOA fluxes (e.g., Loeb et al., 2012). Although the uncertainty in TOA fluxes is also larger than the imbalance inferred from OHC, both Wong et al. (2006) and later Loeb et al. (2012) demonstrated that changes to TOA net fluxes generally track the changes in OHC. It is for this reason that the OHC serves as a constraint on the overall TOA balance. This assertion is supported by recent efforts to track the disposition of energy imbalances within the Earth system that indicate that the combined heat uptake by the atmosphere, land, and cryosphere components of the climate system is more than an order of magnitude less than that absorbed in the oceans (Trenberth et al., 2014). No equivalent data record exists for the net energy balance at the surface and no attempt has been made to examine the extent that the global surface energy balance changes also track OHC changes.

The global mean energy balance requires adjustments to our best estimate of most of the individual fluxes either measured or independently observed. The TOA fluxes are typically adjusted by a few Wm^{-2} to the OHC as mentioned whereas the surface energy balance requires adjustments to our best-estimate of surface fluxes that are much larger. To date these adjustments have been mostly *ad hoc* and have followed two main philosophical approaches. One approach is that of Kiehl and Trenberth (1997) and Trenberth et al. (2009) who assume the most uncertain flux at the surface is the downward longwave radiation (DLR) and apply adjustments principally to this flux, yet no flux uncertainties are given in these studies. The second adjustment approach was introduced by Stephens et al. (2012a) who adjusted the turbulent fluxes of sensible and latent heating arguing these are the most uncertain part of the surface balance based on best-estimate uncertainties. Trenberth et al. adjust the downward longwave radiative flux (DLR) by more 10 Wm^{-2} below our current best estimate of this flux and outside the uncertainty attached to these estimates (Stephens et al., 2012b). By contrast, Stephens et al. adjust the combined latent and sensible heat fluxes upward by more than 10 Wm^{-2} increasing the latent heat flux outside the range suggested by available information on global precipitation (Behrangi et al., 2014). As there is no real evidence to support one adjustment approach over the other, two basic questions then follow. Are there unaccounted for sinks of radiation that could explain why radiant energy incident on the surface might be less than our best estimate of these fluxes? Conversely, are there sources of enhanced precipitation that are missing in current data records?

This paper does not address these two questions specifically as research is ongoing to confront the challenges they represent. Rather the paper provides a review of our current best estimate of the global, annual mean energy balance where the adjustments have been applied more objectively than either of the *ad hoc* methods described above. There have been many such reviews of the Earth's energy balance, including Trenberth et al. (2009), Stephens et al. (2012a, 2012b) as noted, but also recently Stevens and Schwartz (2012), Wild et al. (2013) and L'Ecuyer et al. (in press). While this view of the Earth's energy balance is important in its own right, a much deeper understanding of the Earth's climate system can be gleaned from studies of regional changes in energy balance. The principal focus of the paper is then directed to both the hemispheric and regional character of the energy balance and the influence of the latter on the meridional heat transported poleward.

2. Data resources and methods

2.1. Data

As in Stephens et al. (2012a), all fluxes reported in this paper contain uncertainty estimates, unlike most other energy balance studies of this type. All fluxes have also been adjusted from their original sources but within the context of these uncertainties. From a purely top-of-atmosphere (TOA) perspective, the fluxes contained CERES (Wielicki et al., 1996) in the form of the Energy Budget Adjusted Fluxes (EBAF)[2] (Loeb et al., 2009) are arguably our most authoritative estimate of the TOA balance and we describe important aspects of this balance in the next section. The global average TOA solar irradiance (340 ± 0.1 Wm^{-2}) adopted here are from recent measurements from the Solar Radiation and Climate Experiment (SORCE) (Kopp and Lean, 2011). The adjustments to the TOA outgoing fluxes are performed through the application of a global constraint applied to them as described in Loeb et al. (2009). This constraint comes from independent data on ocean heat content (OHC) available from ARGO data (Lyman et al., 2010). Although restricted to the upper ocean, the recent study of Llovel et al. (2014) provided convincing evidence that these data indeed capture the majority of the total ocean heat content change that has occurred over the past decade. Fig. 1 provides a summary of the EBAF adjustment applied over the past decade, in the form of the total global imbalance of the TOA flux and the hemispheric partitioning of this imbalance. According to these data, the majority of the heat uptake by the oceans occurs in the Southern Hemispheric (SH) oceans, a result also supported the recent analysis of Argo data reported by Roemmich et al. (2015).

The second main source of adjusted flux data are the jointly adjusted TOA and surface fluxes as outlined in the recent study of L'Ecuyer et al. (in press). That study and the companion water cycle analysis of Rodell et al. (in press) applied an objective variational method that imposed joint closure constraints on both the energy and water cycle budgets to derive closed and connected energy and water budgets. This joint water and energy budget depiction combined independent satellite datasets collected between 1998 and 2009 specifically to (i) maximize the availability of modern high quality satellite observations, (ii) use uncertainties of the flux data established for these datasets, and (iii) smooth out interannual variations that may exert a strong influence over shorter intervals. The various datasets employed in this analysis are briefly noted below and additional details concerning their characteristics and the methods used to aggregate them can be found in Rodell et al. (in press) and L'Ecuyer et al. (in press).

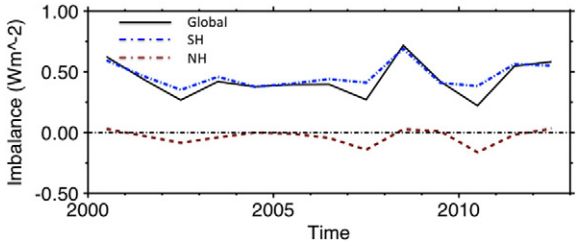

Fig. 1. The global and hemispheric annual mean energy imbalances according to CERES EBAF.

The TOA fluxes are from CERES and the surface flux data sources assimilated by L'Ecuyer et al. include:

(i) SeaFlux Version 1.0 for ocean turbulent heat fluxes through the application of bulk formulas to Special Sensor Microwave/Imager (SSM/I) atmospheric temperature and humidity retrievals using a newly developed neural net algorithm (Curry, 2004; Roberts et al., 2010; Clayson et al., 2015).
(ii) Three independent sources were used to provide estimates of evaporation and sensible heating over land surfaces since these fluxes have large uncertainty. As there is a lack of a clear consensus regarding the superiority of strictly observational approaches and those that integrate such observations using empirical land surface process models, a combination of satellite retrievals and output from global land data assimilation systems was used.
(iii) Independent estimates of atmospheric latent heat release were derived from Version 2.2 of the Global Precipitation Climatology Project (GPCP) monthly Satellite-Gauge precipitation analysis (Adler et al., 2003; Huffman et al., 2009). GPCP integrates observations from geostationary (GEO) and low-Earth (LEO) orbit infrared observations with LEO passive microwave observations from the Special Sensor Microwave Imager (SSM/I) and Special Sensor Microwave Imager and Sounder (SSMIS) and rain gauges over land to generate global, monthly estimates of surface precipitation at 2.5° resolution data.
(iv) The surface radiative fluxes employed here derive from a combination of the International Satellite Cloud Climatology Project Flux Data (ISCCP-FD) (Zhang et al., 2004), and the Global Energy and Water Cycle Experiment (GEWEX) Surface Radiation Budget (SRB) dataset (Gupta et al., 1999; Stackhouse et al., 2001). These datasets calculate surface radiative fluxes based on satellite observations of the spatial distribution of clouds, aerosols, surface albedo, skin temperature, and emissivity constrained with atmospheric temperature and humidity profiles from the Television InfraRed Observation Satellites (TIROS) Operational Vertical Sounder and global atmospheric reanalyses, respectively. The datasets are calibrated to ensure that their simulated TOA fluxes are consistent with CERES observations.

2.2. Data uncertainties

Since the variational approach used to combine fluxes hinges on explicit estimates of the uncertainties in all component fluxes, special attention was given in NEWS to establish these uncertainties. This effort yielded surface radiative flux uncertainties that are similar to those reported in Stephens et al. (2012a). They were established using a combination of sensitivity studies, evaluation against direct radiation measurements, and comparisons against three independent radiative flux datasets as in Stephens et al. (2012a) including the International Satellite Cloud Climatology Project Flux Data (ISCCP-FD) (Zhang et al., 2004) and two new A-Train radiative flux products, CloudSat's 2B-FLXHR-LIDAR dataset and the CALIPSO, CloudSat, CERES, and MODIS (CCCM) merged dataset (Henderson et al., 2013; Kato et al., 2011). While uncertainties in CERES global annual mean net outgoing radiation may be as large as 4.4 Wm^{-2} (Lin et al., 2008), 2σ random errors in monthly mean TOA radiative fluxes from each of these products are expected to be less than 5 Wm^{-2} and these data have been shown to provide a very stable long-term reference as noted. At the surface, sensitivity studies and comparisons against Baseline Surface Radiation Network (BSRN, Ohmura et al., 1998) suggest that regional monthly mean bias errors in the downwelling longwave and shortwave radiation datasets are typically less than 10 Wm^{-2} resulting from uncertainties in lower tropospheric humidity and cloud properties (e.g., L'Ecuyer and Stephens, 2003; Zhang et al., 2007; Stephens et al., 2012a).

Uncertainties in SeaFlux latent and sensible heat fluxes were taken to be 9% and 18%, respectively, based on the combination of sensitivity studies, comparisons against in situ observations, and comparisons against other satellite-derived products described in Roberts et al. (2010) and Clayson et al. (2015). Uncertainties in turbulent heat fluxes over land were estimated from the standard deviation of the three independent datasets that were averaged to generate them. As noted above, these fluxes are the least accurately constrained by satellite observations resulting in uncertainties of 10% and 23% in land-based latent and sensible heat fluxes, respectively. Uncertainties in the core monthly GPCP merged product reflect errors in high quality microwave observations, sampling biases, and uncertainties in gauge-adjustments over land over land. On large scales, uncertainties in GPCP version 2.2 precipitation estimates are taken to be 9% based on the analysis of Adler et al. (2012) which is also similar to that adopted by Stephens et al. (2012b).

None of the flux uncertainties adequately reflect likely biases in the fluxes and various studies attempt to address these. For example, the solar flux incident on the Earth's surface may be biased slightly too high since the effects of unaccounted for absorption by absorbing aerosol cannot be discounted. These biases, however, are likely to be less than a few Wm^{-2} (e.g., Stephens et al., 2012a). Likewise, precipitation estimates inherent to the surface latent heat flux may also be biased low due to missing modes of light precipitation (e.g., Behrangi et al., 2014) or from precipitation inadequately sampled over rugged terrain among other possibilities. Biases in near-surface air temperature and humidity, diurnal sampling corrections, and the parameterization of bulk exchange coefficients can all introduce structural biases in surface heat fluxes (e.g., Gulev et al., 2007a, 2007b; Jimenez et al., 2011; Mueller, 2011; Josey et al., 2014). Addressing these biases are central to answering the two questions posed above.

3. The global-annual mean energy balance

Fig. 2 depicts the annual and global mean energy budget for the first decade of the 21st century obtained using the datasets described. Since a different adjustment has been applied to the CERES TOA fluxes by L'Ecuyer et al. than is applied to produce the CERES EBAF fluxes, both sets of TOA fluxes are included for reference. This provides some sense of the sensitivity of the TOA fluxes to the adjustment process itself. For similar reasons we also include the CERES EBAF 2.7 surface radiative fluxes (e.g., Kato et al., 2011, 2013) to contrast against the NEWS adjusted fluxes. We also provide a second set of adjusted surface fluxes where one of the fluxes (the DLR) is constrained more tightly than is perhaps justifiable to the GEWEX SRB value that is based on a combination of satellite and surface data (Stackhouse et al., 2011) and is practically identical to the CERES EBAF flux value that is also given for reference. Comparison of these values offers some measure of the sensitivity of the remaining surface fluxes to assumptions about the degree of adjustment to one specific flux.

While the general character of the energy balance presented in this figure is well known, the uncertainties are not. The global average TOA solar irradiance (340 ± 0.1 Wm^{-2}) is balanced by 100 ± 4 Wm^{-2} according to CERES or 102 ± 4 Wm^{-2} according to L'Ecuyer et al. study and 240 ± 4 Wm^{-2} of outgoing longwave radiation (OLR) or 238 ± 4 Wm^{-2} respectively in the L'Ecuyer et al. study. The CERES planetary albedo is 0.29 (0.3) and a global emitting temperature is 255 (254.5 ± 0.5) K. From a historical perspective, these values agree with the early estimates from Nimbus 3 observations reported more than four decades ago by Vonder Haar et al. (1972) (0.29 and 254 K) although the present estimates can be considered to be more precise.

Energy fluxes between the atmosphere and surface, on the other hand, differ considerably from those reported by Trenberth et al. (2009) and Stephens et al. (2012b). Most notably, the L'Ecuyer et al. estimate of DLR is 8 Wm^{-2} higher than that reported by Trenberth et al. (2009) while latent heating is 7 Wm^{-2} lower than that reported by Stephens et al. (2012a) or 6 Wm^{-2} lower when the DLR is

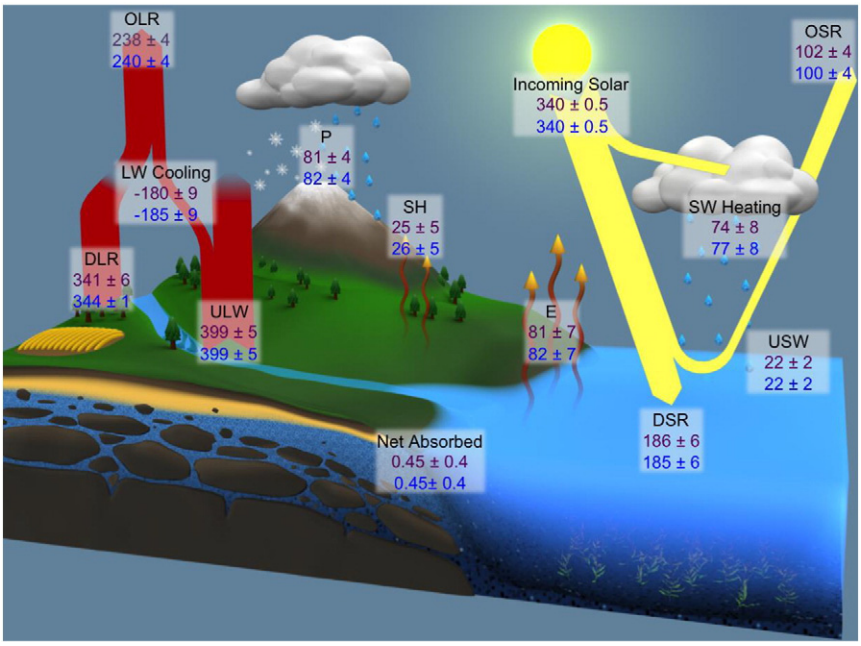

Fig. 2. The global and annual mean Earth's energy balance derived from various sources of data that have been optimized to define closure (refer to text). Two versions of energy balance are provided as an indicator of how the balance can change under different optimization. All quantities are fluxes in units of Wm^{-2}. The gray numbers are the optimized fluxes after L'Ecuyer et al. (in press). The fluxes in blue are from second optimization where the TOA fluxes are more tightly constrained to the CERES EBAF version2.7 fluxes that in turn are constrained to independent OHC information (Fig. 1). The surface fluxes in blue are also more tightly constrained to the GEWEX surface radiation flux product (note the DLR flux difference).

constrained to the 345 Wm^{-2} value. Thus the optimization that takes into account the water balance places the surface energy balance somewhere between that of Stephens et al. and Trenberth et al.

4. Hemispheric balances

Fig. 3 offers a perspective on the hemispheric energy budget of Earth. Although this perspective has been discussed by Stevens and Schwartz (2012) and more recently by Loeb et al. (submitted for publication) and Donohoe et al. (2013), our understanding of it is less certain than

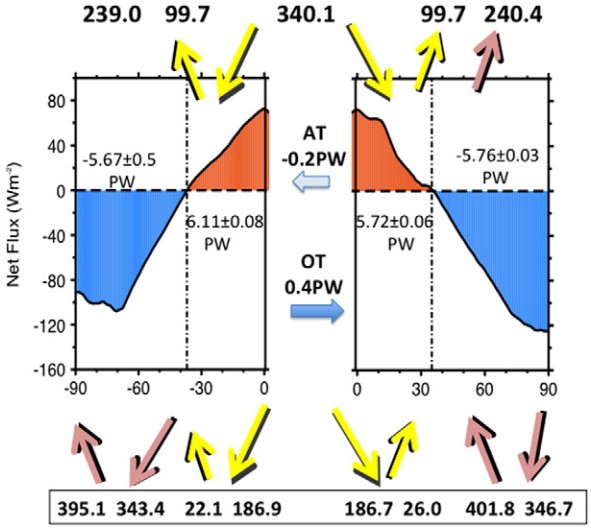

Fig. 3. The annual-hemispheric mean energy balance of Earth. Unless specified otherwise, all TOA and surface numbers are in Wm^{-2}. Fluxes of sunlight entering and leaving the TOA and surface are in yellow and infrared fluxes are red. No hemispheric surface turbulent fluxes are given.

our understanding of the global balance provided in Fig. 2. The TOA fluxes quoted are taken from EBAF directly since the continental flux estimates supplied by L'Ecuyer et al. (in press) do not map well into hemispheric means and hemispheric mean turbulent fluxes equivalent to those of Fig. 2 are generally unavailable. The surface fluxes given at the bottom of the figure are also those from the CERES EBAF surface flux archive. The figure also presents the zonally averaged net TOA flux for reference with this zonal flux profile being separated at the equator for clarity. The amount of heat stored in the lower latitudes of each hemisphere and lost at the respective higher latitudes is also given (in PW). The remarkable result provided in this figure is that the two hemispheres have an almost identical TOA energy balance while the surface radiative fluxes are much more asymmetrical. At the TOA, the SH is slightly out of balance as a result of a small amount of heat being absorbed by the southern oceans (Fig. 1) whereas the NH appears to be balanced. This small hemispheric difference results from a small asymmetry in the OLR as both the incoming solar and reflected solar are identical in both hemispheres (e.g., Vonder Haar and Suomi, 1969; Voigt et al., 2013; Stephens et al., 2015). The slight energy imbalance between the hemispheres implies a net transport of heat across the equator from the warmed SH to the NH. That the NH is warmer in the annual mean than the SH (e.g., Kang et al., 2014) is reflected in the differences in surface longwave flux with the NH emitting almost 7 Wm^{-2} more radiation into the atmosphere from the warmer NH surface. The hemispheric temperature contrast is responsible for an atmospheric transport of heat about 0.2 PW from the NH to the SH. The additional heat absorbed in the SH oceans, together with this cross equatorial transport from the atmosphere, induces an oceanic transport of 0.4 PW from the SH to the NH (Marshall et al., 2013).

Fig. 4a and b provides additional insight on the factors that establish the near hemispheric symmetry in energy balance. Fig. 4a is taken from Stephens et al. (2015) and shows the NH–SH differences in reflected flux and the contributions of this reflected flux by atmospheric scattering processes and surface reflection processes for both all-sky and clear sky fluxes. The details of how these component contributions are determined are described by Donohoe and Battisti (2011) and further outlined

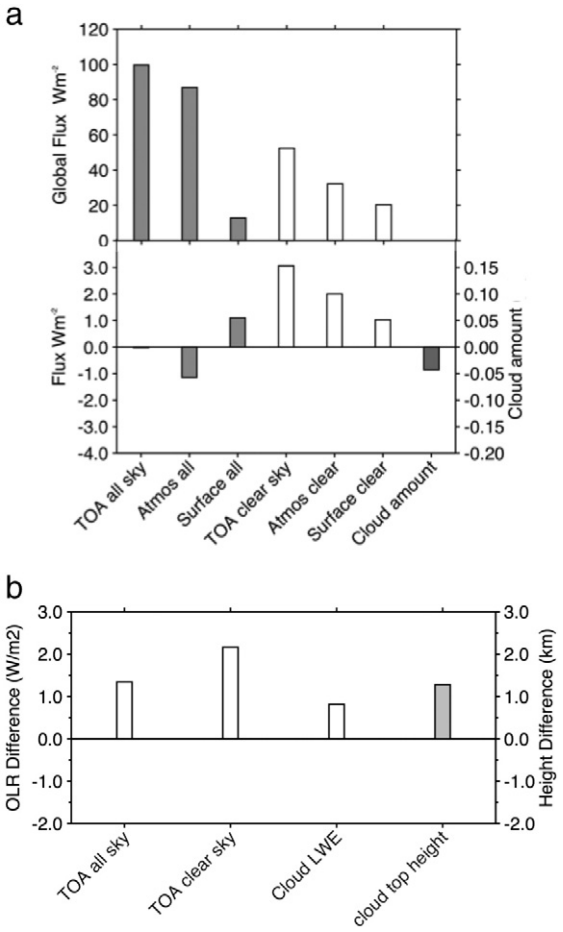

Fig. 4. a (upper) The all-sky and clear-sky global, annual mean reflected fluxes (upper) separated into the two main components. The lower panel of (a) shows the difference between hemispheric annual mean all and clear-sky reflected fluxes and the individual components that comprise these fluxes. These hemispheric differences are defined as the NH minus SH and the all-sky difference is 0.05 Wm^{-2}. Also presented for reference is the hemispheric difference in cloud amount (expressed in absolute units). (b) The NH–SH difference in clear sky and all sky OLR (in Wm^{-2}). The NH being warmer emits more radiation than the SH but this is compensated for by less emission from clouds as indicated by the positive NH–SH difference in cloud longwave effect (Cloud LWE). The NH–SH difference in hemispheric mean cloud top height (in km) based on 4 years of CloudSat-CALIPSO data is also shown for reference.

in Stephens et al. (2015). It is remarkable that the larger surface reflection of the NH is precisely offset by the increased scattering from the SH atmosphere. The latter is a consequence of the greater amounts of cloudiness that exist in the SH as shown in the hemispheric differences of cloud amount taken from 4 years of CloudSat-CALIPSO lidar/radar data (Mace et al., 2009).

A similar analysis of OLR is presented in Fig. 4b in the form of NH–SH OLR differences of the all sky and clear sky fluxes and the longwave cloud radiative effect (LW CRE). A larger clear sky OLR from the NH is a consequence of the warmer NH compared to the SH but this clear sky emission difference in then offset by a larger NH CRE due to fact that on average clouds are both higher and thus colder in the NH compared to the SH. This interpretation of the hemispheric difference in CRE is again supported by the hemispheric cloud top height differences obtained from CloudSat/CALIPSO observations that show the NH clouds to be over 1 km higher than SH clouds.

The results of Fig. 4 are quite remarkable. They show how the near hemispheric symmetry in TOA energy balance is established by hemispheric differences in cloud radiative properties that work to reduce the asymmetries apparent in surface fluxes. The fundamental importance of this cloud regulation of the energy balance between hemispheres to our understanding of the climate system is not fully known. The hemispheric symmetry/asymmetry in energy balance that results also fundamentally dictates how much heat is transported across the equator from one hemisphere to another (Hwang and Frierson, 2013).

The connection between TOA energy balance and cross equatorial heat transfer can be simply demonstrated with the following analysis. Consider the planet composed of two zonally-averaged boxes. In a steady state, each box neither gains nor loses energy, so the net energy flux of radiation N_i into the top of the ith box ($i = 1,2$) must balance the divergence of energy X_i associated heat transported through the sides of the box by the atmosphere and oceans. Thus,

$$N_i + X_i = 0 \tag{1}$$

where

$$N_i = S_i(1-R_i) - L_i \tag{2}$$

and $S_i(1 = R_i)$ is the net shortwave (solar) radiation entering at the top of the atmosphere and L_i is the OLR. For the planet in steady state

$$\sum_i N_i = 0 \tag{3}$$

and because the flux of energy carried by the fluid across the boundaries of one box is gained by its neighbors,

$$\sum_i X_i = 0 \tag{4}$$

as required by (Eq. (1)). For the special case of $X_1 = X_2 = 0$, it then follows that L1 = L2 and $S_1(1 - R_1) = S_2(1 - R_2)$. That is a symmetric energy balance implies a zero cross equatorial heat transport. For the present day Earth, $S_1 = S_2$ and $(1 - R_1) = (1 - R_2)$.

The amount of cross equatorial heat transport, and thus processes that establish it, are also central to determining a number of other important properties of the climate system. Paleo-proxy records, for example, suggest that the mean latitude of the Atlantic ITCZ varies synchronously with North Atlantic climate over a range of timescales throughout the Holocene and Last Glacial Maximum (Chiang et al., 2003; Peterson et al., 2000). Model simulations also reveal that the ITCZ moves south when the NH is forced with the introduction of additional cooling imposed on it (Broccoli et al., 2006). These results, together with other studies with simple models showing effects of southern ocean clouds on the position of the ITCZ (Frierson and Hwang, 2012), suggest that there are indeed extra-tropical influences on the position of the ITCZ and these influences are played out through heat transport across the equator.

Donohoe et al. (2013) argue that a robust, empirical relation exists between the heat transported across the equator, X_{eq}, and the zonal location of the ITCZ across a myriad of timescales. This relation has the approximate form

$$\mathrm{ITCZ}_{loc} \approx -3\left(^{o}\mathrm{PW}^{-1}\right) X_{eq} \tag{5}$$

where the negative sign means the ITCZ location in the NH (+) requires a southward heat flux across the equator. The relationship argues that a northward shift of the ITCZ of 3° is associated with a 1 PW transport southward and away from the hemisphere to which the ITCZ has moved. Conversely, processes that lead to a change to the energy balance in one hemisphere, say of an amount ΔN_1, induces a shift in the heat transport across the equator of ΔX_1 according to Eq. (1) and thus a shift in the ITCZ. The relation (5) explains how the radiative properties of the remote southern ocean clouds, for example, can influence the ITCZ in the opposite hemisphere (Hwang and Frierson, 2013).

5. Meridional heat transport

The differential heating between the lower latitudes and the higher latitudes drives a global heat engine that moves heat poleward via the oceanic and atmospheric circulations. The gross properties of the annual mean meridional heat transport follow from the details of the zonally averaged annual mean net TOA fluxes as highlighted in Fig. 5. Fig. 5a is the zonal profile of absorbed solar and OLR and Fig. 5b is the zonal averaged net TOA flux repeated from Fig. 3. The latitudes where the absorbed solar matches the OLR (36.9 ± 0.2 S, 35.0 ± 0.9 N), indicated by the vertical dashed lines, are the latitudes of zero net TOA flux and are thus the latitudes of maximum heat transport of each respective hemisphere. The latitude of maximum net TOA flux occurs at the equator or very near it, and is also the latitude of zero meridional heat flux. The zonal averaged TOA net flux of Fig. 5b highlights the equatorial regions of positive net flux and extra-tropical regions of negative net flux. The respective amounts of heat gained and lost in these regions calculated from the area weighted net fluxes were given in Fig. 3 with the error bars quoted being an indicator of the interannual variability of these integrated fluxes based on 14 years of CERES EBAF data. It is also noteworthy that the amounts of heat loss from the extra-tropics are very close to the same in each hemisphere (5.7 ± 0.02 PW for the SH, 5.8 ± 0.001 for the NH) and thus the maximum annual mean heat transport by each hemisphere is almost the same, reflecting the near symmetry of the energy balance.

Fig. 6 illustrates a novel analysis of how different components of the radiation balance contribute to the heat accumulated in the southern and northern low latitudes and to the heat lost at the higher latitudes of each hemisphere. In this way the components of the net flux, and processes that influence them, can be interpreted in terms of heat transport. At low latitudes the heat gain mostly occurs as a result of the excess clear-sky absorbed solar radiation over the clear-sky emitted longwave radiation. Net cloud effects in the tropical region as defined by the latitude ranges described above are smaller and negative due to a shortwave cloud effect that compensates longwave cloud effects. The heat loss that occurs in the extra-tropics reveals interesting but expected differences between the hemispheres. For both regions, the longwave emission to space from clear skies exceeds the absorbed solar radiation making the net effect of clear skies negative. The net effects of clouds in higher latitudes are also negative and of a similar magnitude to the clear sky loss. The cloud effects are mostly influenced by the solar effects of clouds, the latter being larger in the SH than the NH.

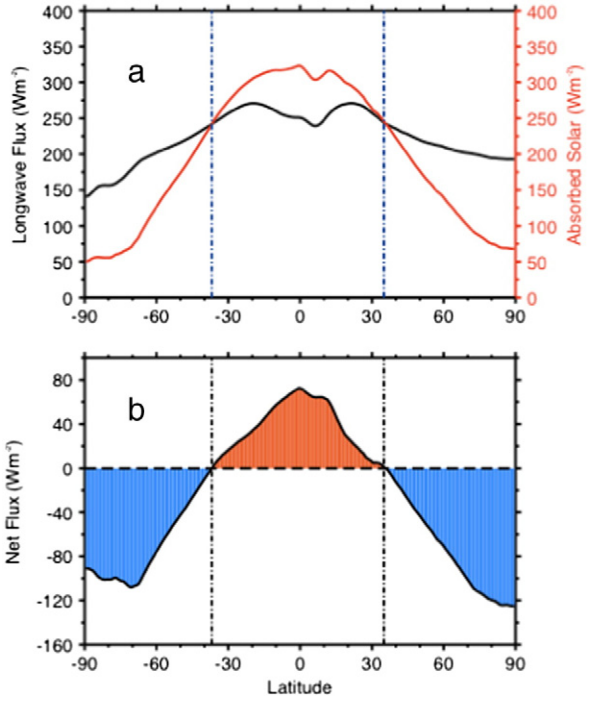

Fig. 5. (a) The CERES EBAF annual mean zonal profiles of absorbed solar and OLR (b) The zonal profile of annual mean net flux repeated from Fig. 3. The latitudes of zero net flux are identified by the vertical dashed lines.

6. Seasonal properties

The seasonal properties of the Earth's energy balance also fundamentally influence regional climate and its variability. Fig. 7 presents the seasonal cycle of storage of energy into the Earth calculated from the 14 year average of CERES EBAF fluxes. The figure presents the seasonal cycle of TOA net flux as a function of latitude. Noteworthy is the way the region of positive energy storage, as defined by positive net TOA flux, swings across the equator from the summer season of one hemisphere to the summer season of the other hemisphere. Also noteworthy are the hemispheric differences in this storage with maximum values of net flux occurring during the summer of the Southern Hemisphere (SH). Less obvious but also important are the smaller net fluxes in the wintertime SH compared to the wintertime northern Hemisphere (NH). As we will show below, these hemispheric asymmetries are principally a consequence of the greater amounts of solar energy incident into the summer SH compared to the summer NH and conversely less solar incoming in the SH winter season.

If the meridional transport is to be computed for times other than the annual mean for which heat storage within the system can be considered to be small (approximately 0.6 Wm^{-2}), the local heat storage of the atmosphere and oceans must be accounted for. The atmospheric contribution to this storage is small whereas the seasonal ocean storage is substantial. Since data on the seasonal cycle of local ocean heat storage are at present lacking, we adopt the method introduced by Riehl and Simpson (1979) to infer seasonal transports from seasonal TOA radiation data. This requires that the heat transport deduced from CERES TOA data at times when the ocean temperatures are at their maxima or minimum since this implies the ocean heat storage is near zero at these times. As Riehl and Simpson (1979) note, these times occur near the end of August and February and transports determined then can be considered to be representative of transport for longer seasonal periods, namely the summer and winter seasons. A test of this assertion lies in the average of the two transports calculated at these times as they ought to represent the annual mean transports when averaged together (Reihl and Simpson, 1979).

The poleward transports of heat at the end of February and August were calculated from the averages of the February and March and August and September CERES net fluxes respectively. These transports are shown in Fig. 8a and b and a few notable features warrant comment. While the annual mean transport exhibits a high degree of symmetry (Fig. 8a), the seasonal transport has much less symmetry. The cross equatorial seasonal transport is also large, 5.3 PW in February and 6.4 PW in August indicating a large transport from the NH to the SH in the Austral winter. The transport is also much more asymmetric in this season compared to the Boreal winter season. The average of the two transports also very nearly reproduces the annual mean transports as the earlier study of Riehl and Simpson (1979) find thus confirming the assumptions of their approach.

The latitudes of zero transport, considered to be the latitudes that delineate the equatorial trough by Reihl and Malkus, are also noted on the figure. These latitudes, determined to be 12.9 S and 19 N from the average of 14 years of CERES data (Fig. 8b), represent the dividing line between where the energy is transported to the summer and winter poles in each season and define the region of the tropical trough zone (TTZ). An interpretation of the TTZ is as follows. During the southern winter season, the winter hemisphere extends from the South Pole to 19 N; conversely during the northern winter season, the winter hemisphere extends from the North Pole to 12.9 S. The TTZ therefore defines

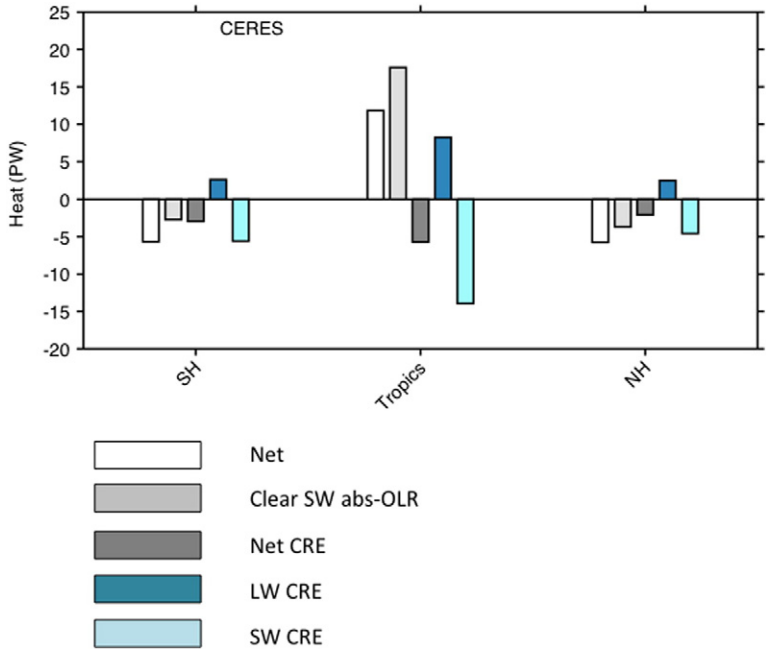

Fig. 6. The components of the annual-mean net flux for the tropical zone identified as the positive net flux zone in Fig. 3 (37 S–35 N) and the two extra-tropical zones of negative net flux. Units are PW and CRE is the cloud radiative effect defined as the difference between clear sky minus all sky outgoing fluxes.

a low-latitude zone where heat is always transported out of that zone toward the winter hemisphere.

The TTZ is not symmetric about the equator extending further into the NH than the SH. The reason for this asymmetry is due to the respective seasonal asymmetries in the amounts of heat both input into the respective summer hemispheres and lost to space by the winter hemispheres. These seasonal asymmetries are further emphasized in Fig. 9 in the form of NH–SH differences in zonally averaged net flux and NH–SH components of the net flux expressed in PW. These differences are formed from the January and July zonal profiles of fluxes taken to be representative of respective summer and winter seasons. The zonally averaged data have been transposed such that the summer pole lies to the right of the figure and the winter pole to the left. The net flux of the SH winter is less than that of the NH winter over much of the hemisphere except in the polar latitudes. As a result, the SH loses about 3.2 PW more heat in it its winter season than does the NH in winter.

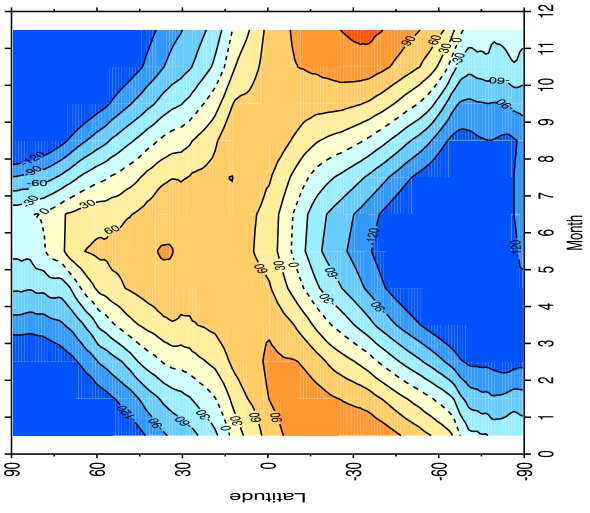

Fig. 7. Heat storage of the Earth–atmosphere system according to a 14 year average of CERES TOA net flux (in Wm^{-2}) as a function of latitude and season.

The main source of this asymmetrical heat loss is the differences in solar radiation incident on each winter hemisphere as evident in the component analysis of Fig. 9. The SH winter receives about 4.4 PW less incoming solar radiation than the NH during winter with the net imbalance being slightly compensated for by about 1.1 PW of increased heat loss from the NH associated with larger amounts of reflected sunlight in the NH winter season presumably from NH land masses.

While the SH winter hemisphere loses more heat than the NH winter, the SH summer hemisphere gains about 5.3 PW more heat than the NH summer hemisphere again mostly as a consequence of the greater amounts of sunlight received by Earth in January than in July. The eccentricity of Earth's orbit is responsible for 6.75 PW of

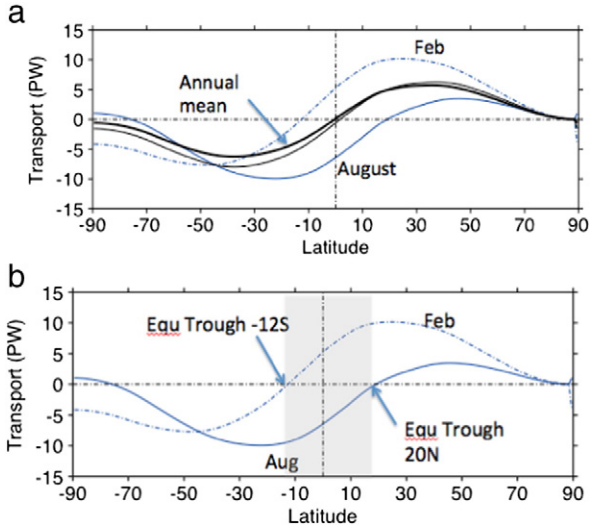

Fig. 8. The late February and August seasonal total heat transport: (a) shows the seasonal transports as highlighted and their average (thin solid line) contrasted against the heavy solid line representing the 14 year annual mean. The slight non-zero transport at the SH pole for both is indicative of the heat gained by the system. (b) The seasonal transports as in (b) highlighting the Tropical Trough Zone (TTZ) as a gray shaded region between 12 S and 20 N.

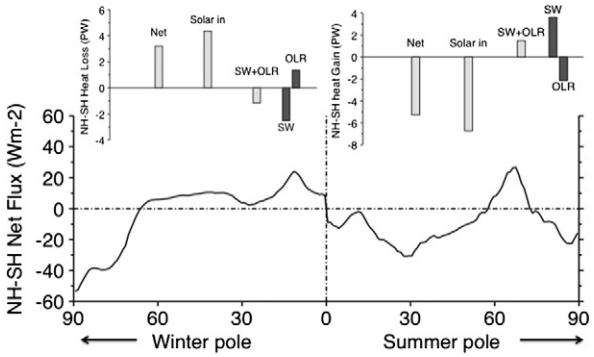

Fig. 9. The NH minus SH winter and summer seasonal differences in net flux and the hemispheric differences in the components of the energy stored in each hemisphere. These differences are derived from July and January TOA fluxes and presents with the summer pole to the right. The component differences shown in the form of histograms and in the winter hemisphere positive values imply greater losses of energy from the SH compared to the NH winter whereas the negative values of the summer components imply increased storage by the SH compared to the NH summer.

extra heat absorbed by the SH during summer compared to that absorbed by the NH in summer. This extra heat is slightly reduced by larger losses of solar energy from the greater amounts of clouds in the SH during summer.

7. Summary

This paper reviews the status of our understanding of the Earth's annual, global mean energy balance, the hemispheric balances and symmetry observed about the equator, and explores the influence of latitudinal changes of energy both on the annual mean and seasonal transports of energy from low latitudes to higher latitudes. The main results of the paper are:

(i) The planet continues to be out of balance with additional heat being added to it at the rate of $0.6 \pm 0.4\ \mathrm{Wm}^{-2}$ which is being taken up by the world's oceans. From the best available information we have, it appears that this heat is primarily entering into the oceans of the SH (Fig. 1, also Roemmich et al., 2015) and perhaps mostly equatorward of 37 S (Fig. 3).

(ii) All representations of the annual mean energy balance, including that provided in Fig. 2, require adjustments to our best estimate of the individual energy fluxes ranging from a few Wm^{-2} at the TOA to more than 10 Wm^{-2} at the surface. To date these adjustments have been performed in an *ad hoc* way. In the present study we report on a balance obtained using more objective constraints on the adjustment process based on best estimate uncertainties of fluxes as given in the study of L'Ecuyer et al. (in press). We contrast these new results against other results for reference and provide some assessment of different assumptions on the impact of the adjustment on the fluxes.

(iii) The energy balances of the Southern and Northern Hemispheres are shown to be practically identical which in turn suggests the transport of energy across the equator in the net also approaches zero. In fact the hemispheres are not identically symmetrical with the SH being slightly out of balance absorbing the additional heat associated with forced climate change (Fig. 1 and 3). The symmetry in absorbed solar and the near symmetry in OLR are remarkable in their own right and are a result of the effects of clouds both on solar reflection and OLR that act to offset land–ocean hemispheric differences (Fig. 4).

(iv) The clear-sky exchanges of energy to space are the dominant processes that shape the properties of the meridional heat transport (Fig. 6). At low latitudes, the excess absorbed solar radiation over the OLR largely determines how much heat is absorbed at low latitudes whereas the increase emission from higher latitudes dictates much of the heat loss from these regions and thus the required transport to higher latitudes. Although clouds have a more complex influence, one common feature is the shortwave effects of clouds tend to be the more dominant effect on transport in all regions. In the higher latitudes, cloud effects particularly sunlight reflected by clouds, are at least as important as clear sky effects whereas at lower latitudes solar and longwave cloud effects largely (but not entirely) offset.

(v) Finally, we show that there are important hemispheric, seasonal influences on the heat transport that conspire to make the seasonal transports to the respective winter hemispheres lopsided. We introduce the Tropical Trough Zone (TTZ) as in Riehl and Simpson (1979) which is the zone of low pressure out of which heat is always transported to the winter pole. We show that the SH winter loses more heat than the respective NH winter (3.2 PW more) due to the reduced sunlight incident on the SH winter hemisphere. This is responsible for the asymmetric position of the TTZ about the equator which extends further into the NH, and is fundamentally a consequence of orbit eccentricity. The consequence of this greater winter loss from the SH is that proportionally more heat is transported out of the TTZ to the southern winter pole than is transported to the northern winter pole. This additional heat to balance the winter energy loss comes from further into the NH summer. The relevance of these seasonal asymmetries to the climate of Earth, such as to the mean location of the Inter-Tropical Convergence Zone (ITCZ), is under study.

Acknowledgments

This study was supported in part by the NASA Energy and Water Cycle Study (NEWS) program grant NNX15AD13G, by the NNN12AA01C that supports the lead author's research exploiting NASA's A-Train constellation and his involvement as co-chair of GEWEX.

References

Adler, R.F., Huffman, G.J., Chang, A., Ferraro, R., Xie, P., Janowiak, J., Rudolf, B., Schneider, U., Curtis, S., Bolvin, D., Gruber, A., Susskind, J., Arkin, P., 2003. The Version 2 Global Precipitation Climatology Project (GPCP) monthly precipitation analysis (1979–Present). J. Hydrometeorol. 4, 1147–1167.

Adler, R.F., Gu, G., Huffman, G.J., 2012. Estimating climatological bias errors for the global precipitation climatology project (GPCP). J. Appl. Meteorol. Climatol. 51, 84–99.

Allen, M.R., Ingram, W.J., 2002. Constraints on future changes in climate and the hydrological cycle. Nature 419, 224–232. http://dx.doi.org/10.1038/nature01092.

Andrews, T., 2009. Forcing and response in simulated 20th and 21st century surface energy and precipitation trends. J. Geophys. Res. 114, D17110. http://dx.doi.org/10.1029/2009JD011749.

Behrangi, A., Stephens, G., Adler, R., Huffman, G., Lambrigtsen, B., Lebsock, M., 2014. An update on oceanic precipitation rate and its zonal distribution in light of advanced observations from space. J. Clim. 27, 3957–3965.

Broccoli, A.J., Dahl, K.A., Stouffer, R.J., 2006. Response of the ITCZ to Northern Hemisphere cooling. Geophys. Res. Lett. 33, L01702. http://dx.doi.org/10.1029/2005GL024546.

Chiang, J.C.H., Biasutti, M., Battisti, D.S., 2003. Sensitivity of the Atlantic Intertropical Convergence Zone to Last Glacial Maximum boundary conditions. Paleoceanography 18 (4), 1094. http://dx.doi.org/10.1029/2003PA000916.

Clayson, C.A., Roberts, J.B., Bogdano, A., 2015. Sea flux version 1: a new satellite based ocean–atmosphere turbulent flux dataset. Int. J. Climatol (in revision).

Curry, J.A., 2004. SeaFlux. Bull. Am. Meteorol. Soc. 85, 409–419.

Donohoe, A., Battisti, D.S., 2011. Atmospheric and surface contributions to planetary albedo. J. Clim. 24, 4402–4418.

Donohoe, A., Battisti, D.S., 2012. What determines the meridional heat transport? J. Clim. 25, 3832–3850.

Donohoe, A., Marshall, J., Ferriera, D., McGee, D., 2013. The relationship between ITCZ location and cross-equatorial atmospheric heat transport. J. Clim. 26, 3597–3618.

Frierson, D.M.W., Hwang, Y.T., 2012. Extra-tropical influence on ITCZ shifts in slab ocean simulations of global warming. J. Clim. 25, 720–733.

Gulev, S., Jung, T., Ruprecht, E., 2007a. Estimation of the impact of sampling errors in the VOS observations on air–sea fluxes. Part I: uncertainties in climate means. J. Clim. 20, 279–301.

Gulev, S., Jung, T., Ru, E., 2007b. Estimation of the impact of sampling errors in the VOS observations on air–sea fluxes. Part II: impact on trends and interannual variability. J. Clim. 20, 302–315.
Gupta, S.K., Ritchey, N.A., Wilber, A.C., Whitlock, C.H., Gibson, G.G., Stackhouse, J.P.W., 1999. A climatology of surface radiation budget derived from satellite data. J. Clim. 12, 2691–2710.
Henderson, D.S., L'Ecuyer, T., Stephens, G., Partain, P., Sekiguchi, M., 2013. A multi-sensor perspective on the radiative impacts of clouds and aerosols. J. Appl. Meteorol. Climatol. 52, 852–870.
Huffman, G.J., Adler, R., Bolvin, D., Gu, G., 2009. Improving the global precipitation record: GPCP Version 2.1. Geophys. Res. Lett. 36. http://dx.doi.org/10.1029/2009GL040 000.
Hwang, Y., Frierson, D., 2013. Link between the double ITCZ problem and cloud bias over southern ocean. PNAS 110, 4935–4940. http://dx.doi.org/10.1073/pnas.1213302110.
Jimenez, C., et al., 2011. Global inter-comparison of 12 land surface heat flux estimates. J. Geophys. Res. 116. http://dx.doi.org/10.1029/2010JD014.
Josey, S.A., Yu, L., Gulev, S., Jin, X., Tilinina, N., Barnier, B., Brodeau, L., 2014. Unexpected impacts of the tropical Pacific array on reanalysis surface meteorology and heat fluxes. Geophys. Res. Lett. 41. http://dx.doi.org/10.1002/2014GL061302.
Kang, S.M., et al., 2014. Croll revisited: why is the Northern Hemisphere warmer than the Southern Hemisphere? Clim. Dyn. 16. http://dx.doi.org/10.1007/S00382-014-2147-Z.
Kato, S., et al., 2013. Surface irradiances consistent with CERES-derived top-of-atmosphere shortwave and longwave irradiances. J. Clim. 26, 2719–2740.
Kato, S., Rose, F.G., Sun-Mack, S., Miller, W.F., Chen, Y., Rutan, D.A., Stephens, G.L., Loeb, N.G., Minnis, P., Wielicki, B.A., Winker, D.M., Charlock, T.P., Xu, K.-M., Collins, W., 2011. Computation of top-of-atmosphere and surface irradiance with CALIPSO, CloudSat, and MODIS-derived cloud and aerosol properties. J. Geophys. Res. 116, D19209. http://dx.doi.org/10.1029/2011JD016050.
Kiehl, J.T., Trenberth, K.E., 1997. Earth's annual global mean energy budget. Bull. Am. Meteorol. Soc. 78, 197–208.
Kopp, G., Lean, J.L., 2011. A new, lower value of total solar irradiance: evidence and climate significance. Geophys. Res. Lett. 38 (1).
L'Ecuyer, T.S., Stephens, G.L., 2003. The tropical atmospheric energy budget from the TRMM perspective. Part I: algorithm and uncertainties. J. Clim. 16, 1967–1984.
L'Ecuyer, et al., 2015. The observed state of the energy budget in the early 21st century. J. Clim. (in press).
Lin, B., Stackhouse, P., Minnis, P., Wielicki, B., Hu, Y., Sun, W., Fan, T.-F., Hinkelman, L., 2008. Assessment of global annual atmospheric energy balance from satellite observations. J. Geophys. Res. 113. http://dx.doi.org/10.1029/2008JD009 869.
LLovel, W., Willis, J., Landerer, F., Fukumori, I., 2014. Deep-ocean contribution to sea level and energy budget not detectable over the past decade. Nat. Clim. Chang. http://dx.doi.org/10.1038/NCLIMATE2387.
Loeb, N.G., Wielicki, B.A., Doelling, D.R., Smith, G.L., Keyes, D.F., Kato, S., Manalo-Smith, N., Wong, T., 2009. Toward optimal closure of the Earth's top-of-atmosphere radiation budget. J. Clim. 22 (3), 748–766.
Loeb, N.G., Lyman, J.M., Johnson, G.C., Allen, R.P., Doelling, D.R., Wong, T., Soden, B.J., Stephens, G.L., 2012. Observed changes in top-of-the-atmosphere radiation and upper-ocean heating consistent with uncertainty. Nat. Geosci. 5, 110–113. http://dx.doi.org/10.1038/ngeo1375.
Loeb, N.G., Wang, H., Cheng, A., Kato, S., Fasullo, J.T., Xu, K.-M., Allen, R.P., 2015. Observational; Constraints on Atmospheric and Oceanic Cross-Equatorial Heat Transport: Revisiting the precipitation asymmetry problem in Climate Models. Clim. Dyn. (submitted for publication).
Lyman, J.M., et al., 2010. Robust warming of the global upper ocean. Nature 465, 334–337.
Mace, G.G., Zhang, Q., Vaughn, M., Marchand, R., Stephens, G., Trepte, C., Winker, D., 2009. A Description of hydrometeor layer occurrence statistics derived from the first year of merged CloudSat and CALIPSO data. J. Geophys. Res. http://dx.doi.org/10.1029/2007JD009775.
Marshall, J., Donohoe, A., Ferreira, D., McGee, D., 2013. The ocean's role in setting the mean position of the Inter-Tropical Convergence Zone. Clim. Dyn. http://dx.doi.org/10.1007/s00382-013-1767-z.
Mueller, 2011. Evaluation of global observations-based evapotranspiration datasets and IPCC AR4 simulations. Geophys. Res. Lett. 38. http://dx.doi.org/10.1029/2010GL046230.
O'Gorman, P.A., Allan, R.P., Byrne, M.P., Previdi, M., 2012. Energetic constraints on precipitation under climate change. Surv. Geophys. 33, 585–608. http://dx.doi.org/10.1007/s10712-011-9159-6.
Ohmura, A., Dutton, E.G., Frohlich, C., Gilgen, H., Hegner, H., 1998. Baseline Surface Radiation Network (BSRN/WCRP), a new precision radiometry for climate research. Bull. Am. Meteorol. Soc. 79, 2115–2136.
Peterson, L.C., Haug, G.H., Hughen, K.A., Rohl, U., 2000. Rapid changes in the hydrologic cycle of the tropical Atlantic during the last glacial. Science 290, 1947–1951.
Riehl, H., Simpson, J., 1979. The heat balance of the Equatorial Trough Zone revisted Contrib. Atmos. Phys. 52, 287–305.
Roberts, J.B., Clayson, C.A., Robertson, F.R., Jackson, D.L., 2010. Predicting near surface characteristics from SSM/I using neural networks with a first guess approach. J. Geophys. Res. 115. http://dx.doi.org/10.1029/2009JD013 099.
Rodell, M., et al., 2015. The observed state of the water cycle in the early 21st century. J. Clim. (in press).
Roemmich, D., Church, J., Gilson, J., Monselesan, D., Sutton, P., Wijffels, S., 2015. Unabated planetary warming and its ocean structure since 2006. Nat. Clim. Chang. 5, 240–245.
Stackhouse Jr., P.W., Cox, S.J., Gupta, S., Chiacchio, M., Mikovitz, J., 2001. The WCRP/GEWEX surface radiation budget project release 2: an assessment of surface fluxes at 1 degree resolution. In: Smith, W., Timofeyev, Y. (Eds.), IRS 2000: Current Problems in Atmospheric Radiation. A. Deepak Publishing.
Stackhouse Jr., Paul W., Gupta, S.K., Cox, Stephen J., Zhang, Taiping, Colleen Mikovitz, J., Hinkelman, Laura M., 2011. The NASA/GEWEX surface radiation budget release 3.0: 24.5-year dataset. GEWEX News 21 (1) (February).
Stephens, G.L., Hu, Y., 2010. Are climate-related changes to the character of global precipitation predictable? Environ. Res. Lett. 5, 025209. http://dx.doi.org/10.1088/1748-9326/5/2/025209.
Stephens, G.L., Li, J., Wild, Clayson, C.A., Loeb, N., Kato, S., L'Ecuyer, T., Stackhouse Jr., P.W., Andrews, T., 2012a. An update on Earth's energy balance in light of the latest global observations. Nat. Geosci. 5, 691–696.
Stephens, G.L., Wild, M., Stackhouse Jr., P.W., L'Ecuyer, T., Kato, S., Henderson, D.S., 2012b. The global character of the flux of downward longwave radiation. J. Clim. 25 (7), 2329–2340 (April 2012).
Stephens, G.L., O'Brien, D., Webster, P.J., Pilewski, P., Kato, S., Li, J.-l., 2015. The albedo of Earth. Rev. Geophys. 53, 141–163. http://dx.doi.org/10.1002/2014RG000449.
Stevens, B., Schwartz, S.E., 2012. Observing and modeling Earth's energy flows. Surv. Geophys. 33. http://dx.doi.org/10.1007/s10712-012-9184.0.
Stone, P., 1978. Constraints on dynamical transports of energy on a spherical planet. Dyn. Atmos. Oceans 2, 123–139.
Trenberth, K.E., Fasullo, J.T., Kiehl, J., 2009. Earth's global energy budget. Bull. Am. Meteorol. Soc. 90 (3), 311–324. http://dx.doi.org/10.1175/2008BAMS2634.1.
Trenberth, K.E., Fasullo, J.T., Balmaseda, M.A., 2014. Earth's energy imbalance. J. Clim. 27, 3129–3144.
Voigt, A., Stevens, B., Bader, J., Mauristen, T., 2013. The observed hemispheric symmetry in reflected shortwave irradiance. J. Climate 26, 468–477.
Vonder Haar, T., Oort, A., 1973. New estimate of annual poleward energy transport by Northern Hemisphere oceans. J. Phys. Oceanogr. 3, 169–172.
Vonder Haar, T.H., Suomi, V.E., 1969. Satellite observations of the Earth's radiation budget. Science 163, 667–669.
Vonder Haar, T.H., Raschke, E., Pasternak, M., Bandeen, W., 1972. The radiation budget of the earth–atmosphere system as measured from the Nimbus 3 satellite. Space Res. 12, 491–498.
Wielicki, B.A., Barkstrom, B.R., Harrison, E.F., Lee III, R.B., Smith, G.L., Cooper, J.E., 1996. Clouds and the Earth's Radiant Energy System (CERES): an earth observing system. Bull. Am. Meteorol. Soc. 72, 853–868.
Wild, M., Liepert, B., 2010. The Earth radiation balance as driver of the global hydrological cycle. Environ. Res. Lett. 5. http://dx.doi.org/10.1088/1748-9326/5/2/025003.
Wild, M., Folini, D., Schär, C., Loeb, N., Dutton, E.G., König-Langlo, G., 2013. The global energy balance from a surface perspective. Clim. Dyn. 40 (11–12), 3107–3134.
Wong, T., Wielicki, B.A., Lee III, R.B., Smith, G.L., Bush, K.A., Willis, J.K., 2006. Reexamination of the observed decadal variability of the Earth radiation budget using altitude-corrected ERBE/ERBS Nonscanner WFOV Data. J. Clim. 19, 4028–4040.
Zhang, Y.-C., Rossow, W., Lacis, A., Oinas, V., Mishchenko, M., 2004. Calculation of radiative fluxes from the surface to top-of-atmosphere based on ISCCP and other global datasets: refinements of the radiative transfer model and the input data. J. Geophys. Res. 109. http://dx.doi.org/10.1029/2003JD004 457.
Zhang, Y.-C., Rossow, W., Stackhouse, P., 2007. Comparison of different global information sources used in surface radiative flux calculation: radiative properties of the surface. J. Geophys. Res. 112. http://dx.doi.org/10.1029/2005JD007457.